Advancements in Brushite cement formulations for bone repair

Morilla Espino, C.

Chapter 5: Compositional changes to brushite cements to improve mechanical and antibiotic-delivery properties.

This chapter is based on:

Morilla Espino, C., van der Weerd, L., de Geus-Oei, L. F., & van den Beucken, J. J. (2025). *Open Ceramics*, 100823.

Introduction

The global demand for dental, craniofacial, and orthopedic bone repair and regeneration has grown due to population aging and the increasing incidence of bone diseases and trauma-induced bone defects[1, 2]. For instance, bacterial infections of bone tissue in the form of osteomyelitis or orthopedic implant-related infections account for substantial clinical cases requiring therapeutic interventions annually [3-5]. Especially orthopedic implant-related infections are likely to become a burden in the near future due to the increasing popularity of orthopedic implants and complexity of the involved surgical procedures. In case these bone conditions result in bone defects that do not heal spontaneously, effective treatment strategies are required. For this, the tissue engineering paradigm has emerged as a 'toolbox' to select scaffolds, growth factors, stem cells, or a combination thereof to enhance bone regeneration [6]. Scaffolds, particularly calcium phosphate cements (CPCs), provide a robust scaffold component that can serve as a suitable environment for bone cell migration, proliferation, and differentiation while supporting defect reconstruction and promoting osteogenesis [2]. CPCs are biocompatible, bioactive, injectable, and resorbable, making them especially suitable for complex cranio- and maxillofacial applications where esthetics are critical. Conventional treatments for (local) bone infection extensive debridement combined with prolonged systemic antibiotic administration (via e.g. intravenous injection). However, these treatments often face challenges in terms of complete removal of bacteria and insufficient antibiotic levels at the infection site to effectively kill bacteria [7]. Emerging drug delivery systems utilizing CPCs offer sustained release of therapeutic agents while promoting osteointegration and reducing adverse side effects [7].

CPCs are mainly classified depending on the final product, i.e. apatitic CPCs (aCPCs) or brushite CPCs (bCPCs) [1]. Apatitic CPCs have α-tricalcium phosphate (α-TCP) as the main precursors, and the reaction normally occurs under basic conditions (pH > 4.2) resulting in the formation of apatite with high similarity to bone mineral [8]. However, the degradation of apatitic CPCs in physiological conditions is relatively slow [1, 9]. In contrast, bCPCs have monocalcium phosphate monohydrate (MCPM) and β-tricalcium phosphate (β-TCP) as their main precursors that form dicalcium phosphate dihydrate (DCPD; brushite) as their end-product [9, 10]. Both these types of CPCs have garnered attention for their use in orthopedic and craniofacial surgeries due to their distinctive properties. During their formation process, a CPC paste is obtained that solidifies in seconds to minutes [10]. bCPCs are known for their injectability, self-setting nature, high biocompatibility, osteoconductivity, and resorbability, which make them particularly

suitable for precise applications like craniofacial defect repairs [1, 11]. bCPCs normally form under acidic conditions (pH < 4.2) and at physiological temperature (37°C), making them thermodynamically metastable and appealing for applications requiring material resorption and replacement by new bone [1]. The rapid resorption of bCPCs within the first weeks post-implantation is driven by disintegration, dissolution, and macrophage activity, which facilitates the removal of bCPC crystals and promotes osteoblast-driven bone formation [11].

Despite their appealing premises, bCPCs face several limitations that hinder their broad application. One significant limitation is the short setting time, which limits the time available for surgeons to apply and manipulate the material for adequate bone defect filling during surgical procedures [12]. Furthermore, their injectability is hindered by issues like liquid phase separation during injection [13, 14]. Regarding mechanical properties, their compressive strength of ~1 MPa [10] is much weaker than cortical (~300 MPa; [15]) and even cancellous (~ 1–15 MPa; [16, 17]) bone; this mechanical mismatch limits their application in load-bearing scenarios [18]. To address these challenges, researchers have explored the incorporation of biopolymers such as chondroitin sulphate [19], chitosan [20], gelatine [21], and alginate [22, 23]. These additives, even in small amounts (e.g. less than 1 wt%), have demonstrated improvements in the mechanical properties and anti-washout characteristics of bCPCs [22]. Further advancements include the addition of natural polymers like silk fibroin, which has shown significant potential in enhancing the mechanical properties of bCPCs [24]. Silk fibroin's robust mechanical properties, biocompatibility, and adjustable bioresorbability make it an attractive additive for modifying mechanical properties of bCPCs [24]. Its unique β-sheet structure introduces surface potentials that promote hydroxyapatite (HA) crystallization, mimicking the natural bone environment and improving the molecular, structural, and biological compatibility of the material [24]. In previous work, it was observed that silk fibroin accelerates the transformation of DCPD into HA [25], which could in principle further improve mechanical properties and promote cell growth [26]. More straightforward, also the addition of α-TCP into a bCPC formulation would result in apatite formation and improvements of mechanical properties.

In view of bacterial bone infections, bCPCs are appealing due to their potential as delivery systems for drugs. Their intrinsic micro- and sub-microporous structure makes them appropriate carriers for active therapeutic agents. Consequently, previous work has explored bCPCs for the local delivery of drugs [27], antioxidants [28], growth factors [29], and antibiotics [27], offering a localized and controlled release of these agents [22]. Antibiotics have a pivotal role in the prevention of bacterial infections after any surgical intervention, particularly when applied locally. Notably, the conventional systemic administration of antibiotics has several side effects

and complications. For this reason, utilizing bCPCs as a drug delivery system for antibiotics presents a promising solution, allowing for minimal, localized dosing while reducing systemic exposure [27, 30].

We herein aim to improve the handling and mechanical properties of bCPC by adding α-tricalcium phosphate (α-TCP) and silk fibroin (SF) into bCPC formulations, and explore different bCPC formulations regarding their function as a drug delivery system for the broad-spectrum antibiotic tetracycline (TC).

Materials and Methods

bCPCs preparation

A basic bCPC formulation (monocalcium phosphate monohydrate, MCPM, Sigma-Aldrich, Germany; β-tricalcium phosphate, β-TCP, CaP Biomaterials LLC, United States) was modified by the addition of α-TCP (CaP Biomaterials LLC, United States) in the powder phase. SF was extracted from silk cocoons as described previously [31] and added into the liquid phase, when in liquid form. For the mechanical properties test the SF was also added as microparticles, obtained following the procedure described elsewhere [32], and fibers, obtained after lyophilization [31], and were added in the solid phase of the bCPC. These constituents were used to prepare a range of bCPC formulations (Table 1).

The formulations shown in Table 1 were designed as part of a full factorial experimental setup to systematically evaluate the individual and combined effects of adding α-TCP, SF, and TC on the performance of the bCPCs. Three α-TCP levels (0%, 10%, and 40%) were selected to study its influence on mechanical reinforcement and phase transformation. SF was incorporated at 1.5 wt% [24] based on literature demonstrating its ability to enhance matrix cohesion and strength. TC was added at 50 mg/cm^3 to assess the potential for local antibiotic delivery. The Mβ formulation (lacking α-TCP, SF, and TC) serves as the negative control, while the remaining formulations include all relevant single-variable and combination groups. This design ensures that the impact of each component can be evaluated independently and in synergy. Sample codes follow a consistent logic: "α" refers to α-TCP percentage, "S" to the presence (S1) or absence (S0) of SF, and "T" to the presence (T1) or absence (T0) of TC. For example, α10-S1-T1 represents a formulation with 10% α-TCP, 1.5% SF, and 50 mg/cm^3 TC.

Table 6. Composition of experimental bCPC formulations.

Formulations (L/P=0.35mg/ml of 8wt.% solution of Na_2HPO_4)	***SF proportions (wt.%; added in liquid phase, fibers and microparticles, added in solid phase)***	***Tetracycline proportions (mg/cm^3) (added in liquid phase)***	***Proportions of α-TCP (%) (added in solid phase)***
Mβ	0	0	0
Mβ-S0-T1	0	50	
Mβ-S1-T0	1.50	0	
Mβ-S1-T1	1.50	50	

α10	0	0	10
α10-S0-T1	0	50	
α10-S1-T0	1.50	0	
α10-S1-T1	1.50	50	
α40	0	0	40
α40-S0-T1	0	50	
α40-S1-T0	1.50	0	
α40-S1-T1	1.50	50	

Physico-chemical material characterization

Crystallographic phase characterization was carried out by means of X-ray diffraction, in a Philips X'pert Modular Powder Diffractometer (PANaytical), RU200B diffractometer with Cu-Kα radiation (1.54059 nm). The scans were made in a 2θ angular interval of 10 –40° and scanning speed of 0.02°/min. The results were interpreted using the X'Pert HighScore PANalytical program database, version 3.0 (PANalytical B. V. Almelo, The Netherlands).

Infrared spectra (FTIR) were obtained in a Fourier transform infrared spectrometer Shimadzu IR Tracer 100 (Japan), with a resolution of 4 cm^{-1} and 21 scans per sample in a range of 400-4000 cm^{-1}.

The total porosity of the bCPC formulations was determined by assessing the volume of water contained in the bCPCs pores relative to the total sample volume. The bCPCs were prepared in Teflon cylindric molds of 12 mm height by 6 mm diameter. Once the bCPCs were fully set, the wet samples were weighed. The samples were then completely dried by placing them under vacuum at room temperature for 24 hours. After drying, the samples were weighed again. Porosity was then determined as the ratio of the pore volume (the volume of water removed during drying) to the total sample volume. The pore volume was calculated as the difference between the wet and dry weights, assuming the density of water is 1 g/cm^3. The total volume of the sample was calculated using the formula $\pi r^2 h$. The porosity is then expressed as:

$$Porosity = \frac{Pore\ Volume}{Total\ Volume} = \frac{Wet\ Weight - Dry\ Weight}{Total\ Volume}$$

Handling properties

The setting time of bCPCs was determined using a Gillmore needle protocol according to a voluntary consensus technical international standard (American Society for Testing and Materials; ASTM C266-89). The lighter-weighted needle (100 g in weight and 2 mm in diameter) was used to determine the initial setting time, while the heavy-weighted needle (300 g in weight and 1 mm in diameter) for the final setting time [33]. After the homogeneous paste of bCPC was inserted into the mold, the setting time was quantified by measuring the timepoint when the needles did not make visible indentations anymore in the bCPCs surface.

The injectability of the bCPCs was determined by extruding a certain quantity of the paste placed in a commercial plastic syringe of 3 mL capacity and with an exit diameter in the nozzle of 2 mm. The extrusion was performed by placing the syringe in a universal testing machine (ESM 303, Mark 10, New York, USA) using a compression speed of 15 mm / min until reaching a maximum load of 100 N [34]:

$$Injectability = \frac{\text{mass of injected material}}{\text{total mass of material}} \cdot 100\%$$

Mechanical characterization

The compressive strength of bCPC formulations was assessed as described previously [35]. In brief, samples (12 mm height, 6 mm diameter, n=3) were immersed in water at 37°C and tested after 24h of sample preparation, immediately after being extracted in order to maintain hydration. The study was carried out in a universal testing machine (ESM 303, Mark 10, New York, USA) with a load cell of 200 N at 1 mm min^{-1} load application speed. The compressive strength (σ_c) in MPa was determined by the following formula:

$$\sigma_C = \frac{F}{A_0} = \frac{4P}{\pi d^2} \cdot 10^{-6}$$

where *P* is the maximum breaking load (N) and *d* the diameter of the specimen (m). Three samples were tested for each bCPCs formulation.

Drug release kinetics

bCPC samples (n=3) loaded with tetracycline were immersed in 2 mL of MES buffer (pH 4.6) at 37.0±0.5 °C throughout the study. Samples representing 1 mL of the supernatant were taken and replaced with an equal volume of fresh MES buffer to maintain submerged conditions; sampling was done at 24h, 72h, 120h, 168h and 336h. The concentration of released TC was measured

using a UV-Visible Spectrophotometer SpectraMax® iD3 Multi-Mode Microplate Reader (Molecular Devises, USA) at a wavelength of 276 nm. Results were calculated as cumulative release over time [36].

Antibacterial efficacy

For the evaluation of antibacterial efficacy [37], *Staphylococcus aureus* strain ATCC 29213 Agar Tripton was used at a strain concentration adjusted with a turbidimetric method employing as a reference a 0.5 McFarland standard (1×10^8 CFU mL^{-1}). Subsequently, 200 µL of a previously prepared culture medium of 90922-500G Mueller Hinton Broth 2 agar (Merck) was inoculated in Petri dishes. After a period of 1 hour, the bCPCs samples were placed on top of the plates containing the culture medium and the bacterial suspension and were incubated at 37 ± 1°C for a period of 168h. Three samples were tested for each formulation and the zone of inhibition was measured using APP Interscience scan 500 colony counter (diameters of inhibition zone less than 10 mm were recorded as non-active antibacterial activity [38]).

Statistical analysis

All data are presented as mean ± standard deviation (SD). Statistical analysis was performed using OriginPro 2018 (OriginLab, USA) and GraphPad Prism 8.0.1 (GraphPad Software, USA). Differences between groups were evaluated using one-way ANOVA followed by appropriate post-hoc tests. A p-value < 0.05 was considered statistically significant.

Results

Characterization of constituents, bCPC formulations, and handling properties

SF was used in different forms: dissolved in water, as fibers, and as particles (Figure 1a-c). The liquid SF (Figure 1a) appeared smooth and homogeneous, indicating its suitability for uniform mixing with the bCPCs components, while the SF fibers (Figure 1b) displayed an elongated structure, and the SF microparticles (Figure 1c) appeared irregular. X-ray diffraction (XRD) analysis (Figure 1d) confirmed DCPD (brushite, ICDD PDF 9-0077) as the dominant phase across all bCPC formulations (Mβ, α10, α40). bCPCs exhibited initial setting times between 4 and 7 minutes, and final setting times ranging from 7 to 30 minutes (Figure 1e). The setting time data shows that adding TC and/or SF to the baseline bCPC formulations (Mβ, α10, α40) tends to prolong both initial (Ti) and final (Tf) setting times. FTIR spectra of the bCPCs (Figure 1f) revealed the presence of characteristic phosphate bands $v_3(PO_4^{3-})$ and the double signal of $v_4(PO_4^{3-})$, across all groups, confirming the formation of calcium phosphate phases. Injectability of the bCPC formulations reached values up to 50% (Figure 1g), the α10 group showed significant differences upon addition of TC and SF. Comparisons between α10 and α40 groups also revealed formulation-dependent variability.

Porosity ranged from 39.6% to 49.9% (Figure 1h), and did not differ significantly across groups ($p > 0.05$), suggesting that the addition of SF or TC did not markedly alter the internal microstructure of the set bCPCs.

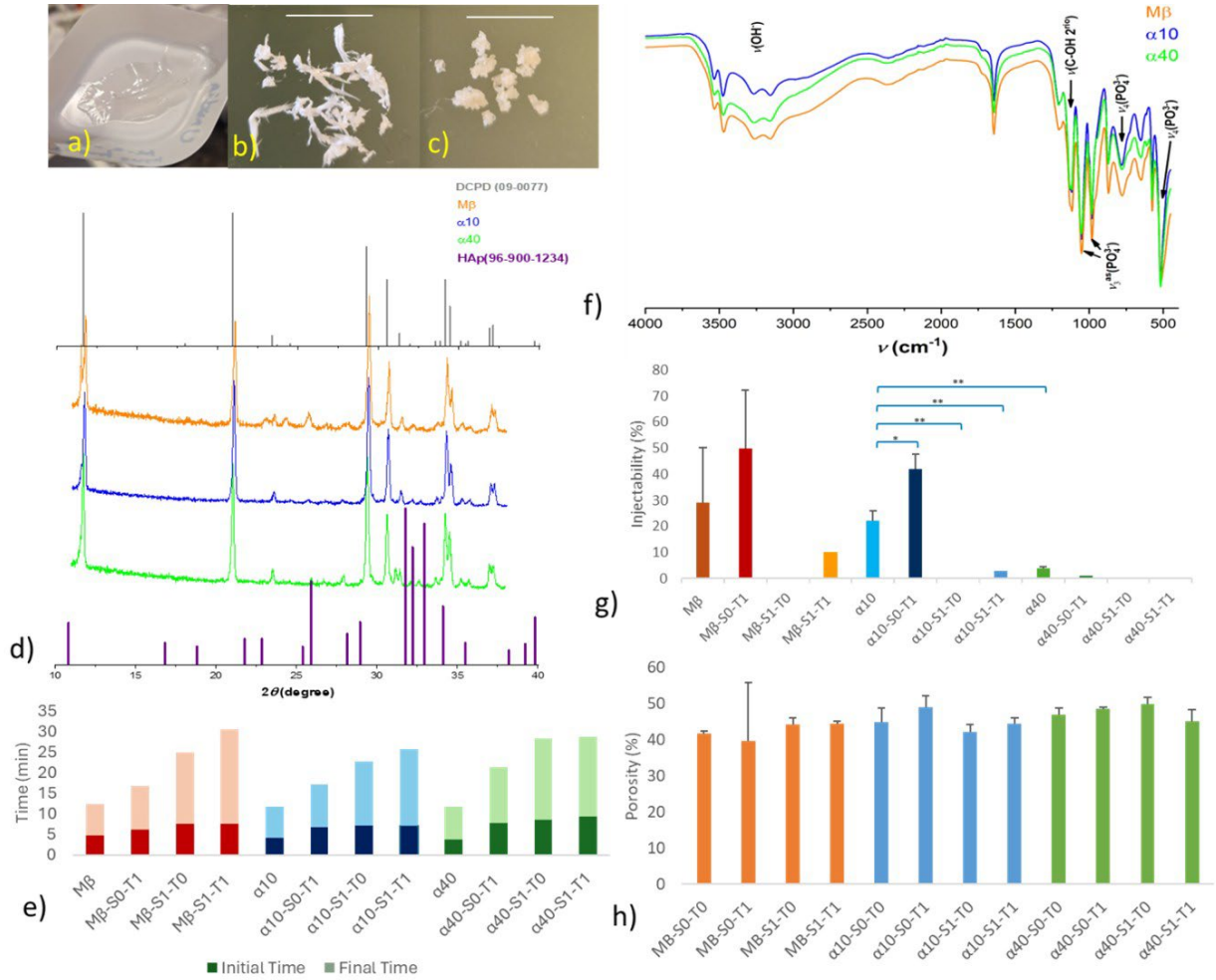

Figure 1. Characterization of constituents, bCPC formulations, and handling properties. *(a) SF liquid. (b) SF fibers (scale bar=1 cm). (c) SF microparticles (scale bar=1 cm). (d) XRD spectra of bCPC formulations and standards (DCPD, ICDD PDF 9-0077; HAp, 96- 900-1234). (e) Initial and final setting times of the bCPC formulations (f). FTIR spectra of the bCPCs (g) Injectability of bCPC formulations (* p<0.05; ** p< 0.01).h) Porosity of the bCPC formulation samples (p>0.05). Statistical significance was determined using one-way ANOVA followed by Tukey's post-hoc test ((* p<0.05; ** p< 0.01).*

Mechanical evaluation of bCPC formulations

Mechanical properties of the bCPC formulations were tested with an experimental set-up (Figure 2a). Macroscopic evaluation of fractured samples (after compressive strength testing) showed presence of SF as fibers or microparticles in the plane of fracture (Figure 2a). The compressive strength of the samples (Figure 2b) showed a range between 0.77 and 2.65 MPa, with statistically significant differences observed in several α10 formulations, were the addition of SF to the samples also containing TC decreased mechanical strength ($p < 0.01$). For the α40 formulations, all additives significantly decreased mechanical strength. Figure 2c displays the correlation between the α-TCP content and the compressive strength. Notably, the inclusion of α-TCP correlated with increased compressive strength. Comparisons between SF forms (Figure 2d)

indicated that SF microparticles reduce compressive strength compared to SF liquid and fibers for α40 formulations, while SF liquid and fibers showed comparable effects on mechanical strength ($p > 0.05$). For Mβ and α10 formulations, no clear effects on mechanical strength were detected upon addition of any type of SF. Overall, the results indicate that α40 formulations outperform Mβ and α10 in terms of compressive strength, and SF microparticles consistently decrease mechanical performance compared to SF liquid and fibers in these formulations.

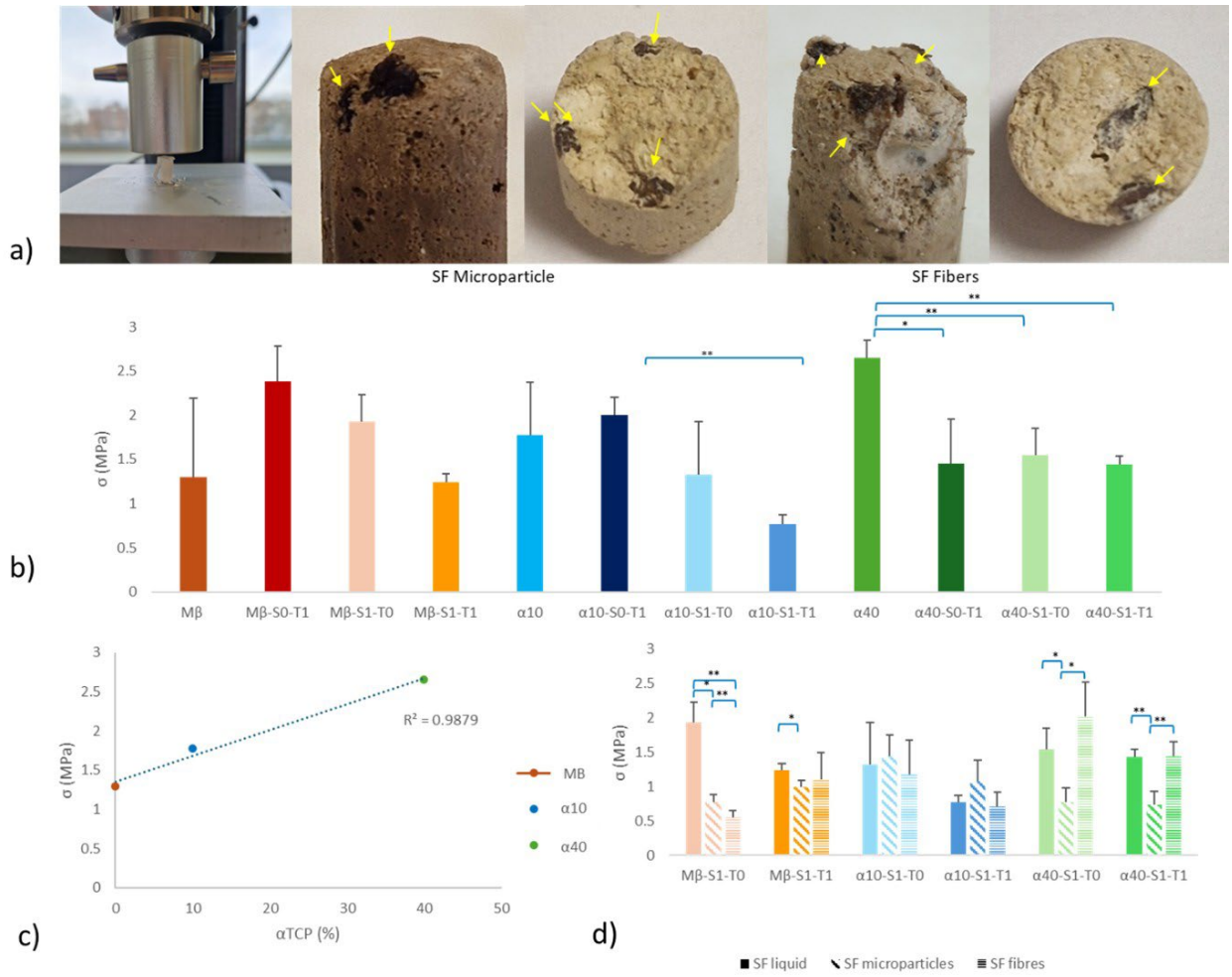

Figure 2. Mechanical properties of bCPC formulations. *(a) Experimental set-up of the test system used for compressive strength evaluation. SF microparticles and fibers were observed at the plane of fracture of samples after compressive strength (yellow arrows). (b) Compressive strength of bCPC formulations (SF in liquid form added in the liquid phase; * = p<0.05; ** = p< 0.01). (c) Compressive strength of bCPC formulations depending on αTCP addition. (d) Compressive strength depending on SF addition in different forms. Statistical significance was determined using one-way ANOVA followed by Tukey's post-hoc test (* p<0.05; ** p< 0.01).*

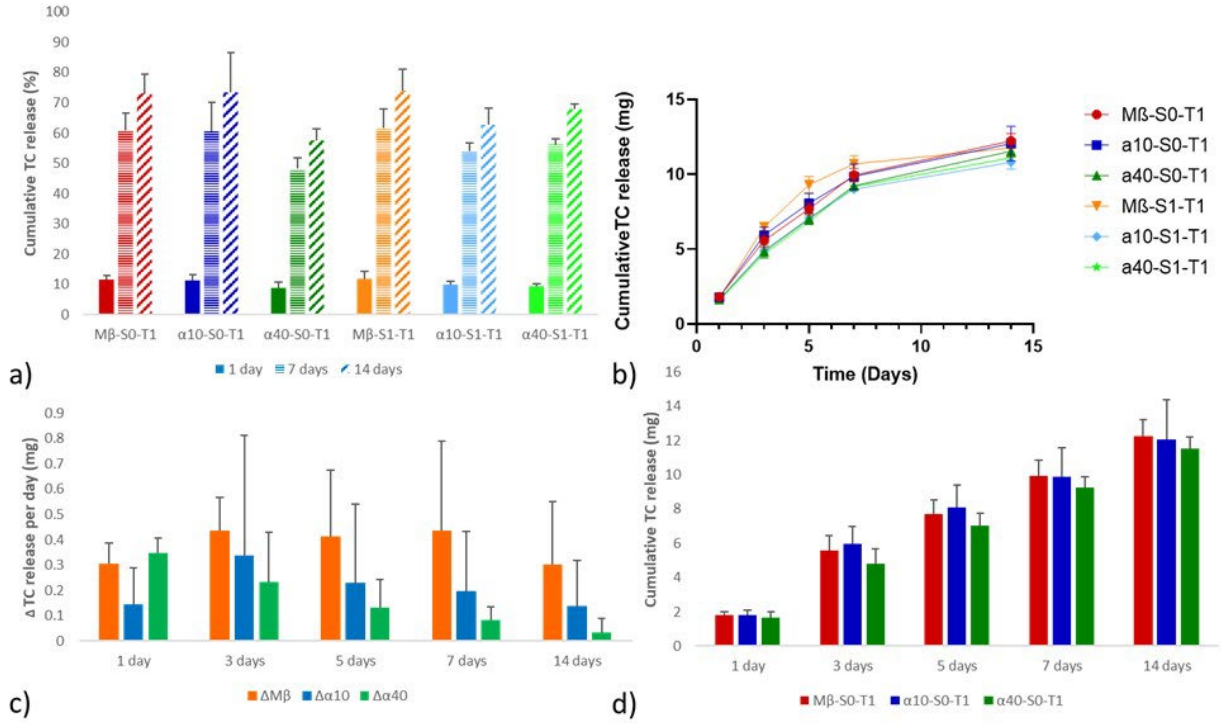

Figure 3. Evaluation of tetracycline release from bCPC formulations. (a) Cumulative TC release (%) after immersion of samples in MES buffer for 1, 7, and 14 days. (b) Cumulative TC release (mg) after immersion of samples in MES buffer for 1, 3, 5, 7, and 14 days. (c) Effects of SF addition on TC release (ΔTC release = release formulation with SF – release formulation without SF; p>0.05). (d) Effects of α-TCP addition on TC release (p>0.05). Statistical analyses were done using a one-way ANOVA followed by Tukey's post-hoc test.

Tetracycline release and antibacterial efficacy

Figure 3a show the cumulative TC release (%) after immersion of samples in MES buffer for 1, 7, and 14 days. On the first day, all samples showed a burst release of approximately 10%. Thereafter, TC release continued to reach approximately 56% in the first 7 days, increasing to approximately 77% cumulative release after 14 days. The release profiles (Figure 3b) show a steady and comparable release profile for all formulations over time. Examination of the influence of SF addition (Figure 3c) indicated no statistically significant differences between groups at any time point (p>0.05). Similarly, the addition of α-TCP (Figure 3d) did not affect TC release across groups (p>0.05).

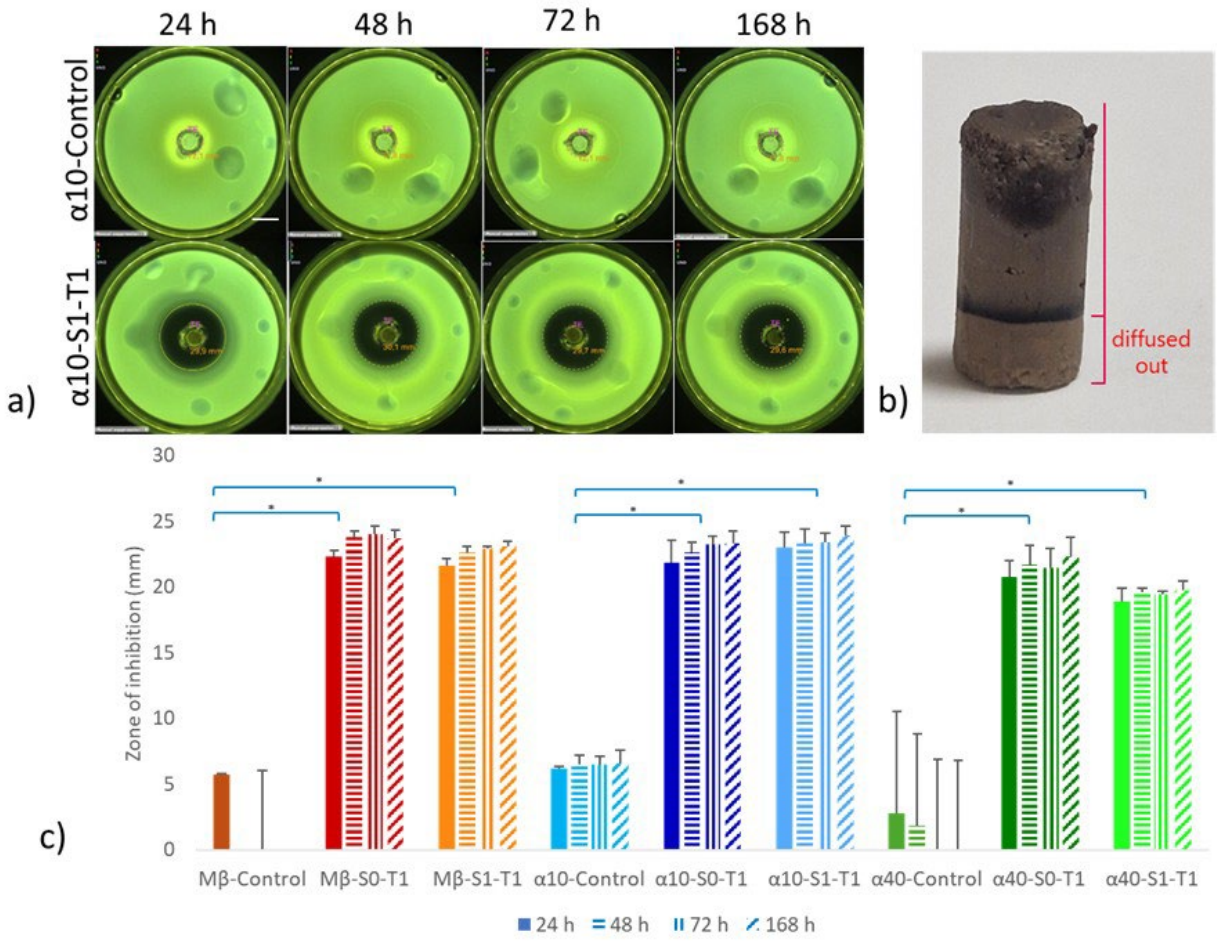

Figure 4. Antibacterial efficacy of bCPC formulations. (a) Representative visual aspect of Zone of Inhibition (ZOI) from α10-S1 samples (+/- TC) over a period of 168h (scale bar=10 mm). (b) Representative α10-S1-T1 sample after 168h showing colour differences along the height of the sample (high in the cylinder the TC remains undiffuse). (c) Quantitative ZOI values against Staphylococcus aureus at 24, 48, 72, and 168 h. Statistical analysis was performed using one-way ANOVA followed by Tukey's post-hoc test. Significant differences between T0 controls and most T1 groups are marked with brackets ($p < 0.05$) in the graph, confirming enhanced antibacterial activity due to TC addition.*

Figure 4 shows the evaluation of antibacterial efficacy of bCPC formulations against *Staphylococcus aureus*. In Figure 4a, the zone of inhibition (ZOI) for α10-S1 samples demonstrates significant antibacterial activity when TC is loaded, with consistent ZOI values observed over time. For α10-S1-T1 samples, the sample cylinder shows a clear line related to TC diffusion, with the top portion of the cylinder visibly darker, indicating undiffused TC (Figure 4b). The ZOI measurements for the bCPC formulations over 24, 48, 72, and 168 hours are displayed in Figure 4c. The controls show negligible ZOI values (<10 mm), confirming no inherent antibacterial effect without TC. In contrast, TC-loaded samples exhibit significantly larger ZOIs (20–25 mm) that remain consistent over time.

Discussion

In this study, we set out to develop a multifunctional bone graft based on brushite calcium phosphate cement (bCPC) that integrates α-tricalcium phosphate (α-TCP) and silk fibroin (SF) with the antibiotic tetracycline (TC) to achieve a balance of mechanical performance and sustained drug release. Our experimental set-up involved characterizing the different forms of SF (liquid, fibers, and microparticles), evaluating setting times, compressive strength, and assessing both drug release profiles and antibacterial efficacy. The main findings were that (i) adding SF and TC significantly prolonged setting times, (ii) adding α-TCP markedly increased compressive strength, and (iii) adding SF in liquid or fiber form reinforced the matrix. For all bCPC formulations, the TC release profile showed an initial burst followed by sustained release over 14 days, and TC-loaded formulations exhibited robust antibacterial efficacy against Staphylococcus aureus.

bCPC formulations clearly showed effects of additives on setting times. Our results indicated that the addition of TC and SF extends both the initial and final setting times of the bCPC formulations. This extended setting time is likely due to TC's ability to chelate calcium ions, thereby delaying brushite crystallization [30, 36]. From a clinical standpoint, these extended setting times can be beneficial, as they allow surgeons more flexibility during implantation [39]. However, overly extended setting times may be impractical in emergency surgical situations, such as cranioplasty [40]. Consequently, specific clinical applications might require individual optimization setting times to strike a balance between workability and efficiency.

Mechanical testing revealed that α-TCP plays a pivotal role in enhancing compressive strength, with bCPC formulations comprising 40 wt% αTCP achieving values up to 2.65 MPa, a 2.65-fold increase over the 1 MPa strength of the unmodified (bare) bCPC [10]. Notably, incorporation of SF in liquid or fiber form resulted in maintained or improved mechanical performance [41, 42], whereas SF microparticles consistently reduced compressive strength—most likely due to irregular shapes acting as stress concentrators [43]. Although prior studies have reported higher compressive strengths for pure α-TCP-based CPC systems [44], the multi-component nature of our bCPC formulations explains the lower absolute values. These observations corroborate recent literature. For instance, Roshanfar *et al.* [41] demonstrated that incorporating electrospun SF fibers into CPC increased compressive strength significantly by bridging microcracks and arresting crack propagation, while discrete polymer particles sometimes served as weak points in the matrix. Similarly, Cassel *et al.* [45] reported that even low concentrations of SF, when well-dispersed, can refine the crystallization of the CPC, resulting in a denser microstructure with enhanced load-bearing capability. These studies support our findings and underscore the

importance of not only the presence but more importantly the form of SF in determining mechanical performance.

TC release profiles demonstrated a predictable burst-sustained release pattern, with approximately 10% release on the first day and up to 77% cumulative release at 14 days. This release profile suggests that the initial burst release is related to diffusion of TC through the intrinsic porosity of the bCPC formulations [27], and corresponds to the Higuchi model [46]. Importantly, neither SF addition nor α-TCP significantly altered TC release kinetics ($p > 0.05$). Antibacterial tests against *Staphylococcus aureus* confirmed the efficacy of the TC-loaded bCPCs, with inhibition zones sustained for up to 168 hours, demonstrating prolonged diffusion of TC out of the cylindrical samples. Comparisons with recent literature further elucidate these findings and bCPCs are known to exhibit burst release due to their high solubility. In studies by Fosca *et al*. [47], pure bCPCs systems were shown to release a majority of their drug payload in a rapid initial phase, whereas incorporating a secondary phase such as HA (or partially converted α-TCP) moderated the burst, shifting the release profile toward a more sustained pattern. Similarly, Rödel *et al*. [21] incorporated gelatin into bCPCs, which transformed the typical burst release into a more prolonged, controlled delivery, following a near-linear release over several days. In work by Dong *et al*. [48], the integration of SF as a hydrogel network moderated the initial burst, allowing for sustained release without compromising mechanical integrity. Our findings align with literature reporting that while bCPC composition impacts initial burst magnitude, the microstructural porosity ultimately controls sustained drug diffusion [23, 30].

Collectively, these results indicate that SF (particularly in liquid or fiber form) and α-TCP can be effectively combined within bCPC matrices to improve both mechanical integrity and therapeutic functionality without negatively affecting drug release behaviour. The observed improvements in compressive strength as well as the predictable, sustained drug release provide a robust foundation for further optimization of bCPC-based drug delivery systems. However, several challenges remain. First, our experiments were conducted exclusively in vitro, which does not fully capture the complexities of the in vivo environment, such as variations in fluid dynamics, local tissue interactions, long-term biodegradation behaviour, and effects of proteins in bodily fluids. In addition, although our data demonstrate clear effects of SF morphology on mechanical properties, the current study does not fully elucidate the optimal size, shape, or distribution of SF microparticles to minimize stress concentration without sacrificing their bioactive benefits. Finally, additional drug-loading strategies should be explored to further enhance and tailor the antibiotic release profile for different clinical scenarios. By integrating these strategies and

leveraging recent advances in multifunctional bCPCs, future research can pave the way for clinically effective, economically viable materials for bone regeneration.

Conclusions

Our study demonstrates that bCPC systems are promising multifunctional platforms for bone regeneration, effectively balancing mechanical strength, injectability, and sustained antibiotic delivery. Incorporating SF (in liquid or fiber form) and α-TCP allows for tuneable setting times and improved compressive strength without compromising porosity or drug diffusion. These effects of integrating these additives in bCPC provide a robust foundation for optimizing bCPC formulations for clinical applications in bone repair. Future studies should focus on in vivo validation, long-term degradation, and advanced drug-loading strategies to expand the therapeutic reach of these biomaterials.

References

[1] K. Hurle, J. Oliveira, R. Reis, S. Pina, and F. Goetz-Neunhoeffer, "Ion-doped brushite cements for bone regeneration," *Acta Biomaterialia,* vol. 123, pp. 51-71, 2021.

[2] Y. Lin *et al.*, "Calcium phosphate cement scaffold with stem cell co-culture and prevascularization for dental and craniofacial bone tissue engineering," *Dental Materials,* vol. 35, no. 7, pp. 1031-1041, 2019.

[3] H. M. Kremers, M. E. Nwojo, J. E. Ransom, C. M. Wood-Wentz, L. J. Melton III, and P. M. Huddleston III, "Trends in the epidemiology of osteomyelitis: a population-based study, 1969 to 2009," *JBJS,* vol. 97, no. 10, pp. 837-845, 2015.

[4] E. Witso, "The rate of prosthetic joint infection is underestimated in the arthroplasty registers," vol. 86, ed: Taylor & Francis, 2015, pp. 277-278.

[5] J. Schimmel, P. Horsting, M. De Kleuver, G. Wonders, and J. Van Limbeek, "Risk factors for deep surgical site infections after spinal fusion," *European Spine Journal,* vol. 19, pp. 1711-1719, 2010.

[6] R. Langer, "I articles," *Science,* vol. 260, p. 5110, 1993.

[7] M. Gallarate, D. Chirio, G. Chindamo, E. Peira, and S. Sapino, "Osteomyelitis: focus on conventional treatments and innovative drug delivery systems," *Current Drug Delivery,* vol. 18, no. 5, pp. 532-545, 2021.

[8] P. Arokiasamy *et al.*, "Synthesis methods of hydroxyapatite from natural sources: A review," *Ceramics International,* vol. 48, no. 11, pp. 14959-14979, 2022.

[9] C. M. Espino, G. F. Estévez, L. van der Weerd, L.-F. de Geus-Oei, and J. J. van den Beucken, "Innovations for Brushite Cements toward applications in Bone Regeneration and Drug Delivery," *Ceramics International,* 2024.

[10] A. A. Mirtchi, J. Lemaitre, and N. Terao, "Calcium phosphate cements: study of the b-tricalcium phosphate - monocalcium phosphate system," *Biomaterials,* vol. 10, pp. 475-480, 1989, doi: 10.1016/0142-9612(89)90089-6.

[11] R. Jayasree, T. S. Kumar, R. Venkateswari, R. P. Nankar, and M. Doble, "Eggshell derived brushite bone cement with minimal inflammatory response and higher osteoconductive potential," *Journal of Materials Science: Materials in Medicine,* vol. 30, pp. 1-14, 2019.

[12] A. C. de Franca Silva Azevedo *et al.*, "Brushite bone cement containing polyethylene glycol for bone regeneration," *Bio-Medical Materials and Engineering,* vol. 33, no. 3, pp. 221-233, 2022.

[13] S. V. Dorozhkin, "Self-Setting Calcium Orthophosphate Formulations," *J. Funct. Biomater,* vol. 4, no. 4, pp. 209-311, 2013, doi: https://doi.org/10.3390/jfb4040209.

[14] A. T. Saleh, L. S. Ling, and R. Hussain, "Injectable magnesium-doped brushite cement for controlled drug release application," *Journal of materials science,* vol. 51, no. 16, pp. 7427-7439, 2016.

[15] T. Weerasooriya, B. Sanborn, C. A. Gunnarsson, and M. Foster, "Orientation dependent compressive response of human femoral cortical bone as a function of strain rate," *Journal of Dynamic Behavior of Materials,* vol. 2, pp. 74-90, 2016.

[16] C. E. Dunham, S. E. Takaki, J. A. Johnson, and C. E. Dunning, "Mechanical properties of cancellous bone of the distal humerus," *Clinical Biomechanics,* vol. 20, no. 8, pp. 834-838, 2005.

[17] L.-C. Gerhardt and A. R. Boccaccini, "Bioactive glass and glass-ceramic scaffolds for bone tissue engineering," *Materials,* vol. 3, no. 7, pp. 3867-3910, 2010.

[18] Q. Liu, W. F. Lu, and W. Zhai, "Toward stronger robocast calcium phosphate scaffolds for bone tissue engineering: A mini-review and meta-analysis," *Biomaterials Advances,* vol. 134, p. 112578, 2022.

[19] F. Tamimi-Mariño, J. Mastio, C. Rueda, L. Blanco, and E. López-Cabarcos, "Increase of the final setting time of brushite cements by using chondroitin 4-sulfate and silica gel," *Journal of materials Science: Materials in medicine,* vol. 18, pp. 1195-1201, 2007.

[20] S. Rattanachan, C. Lorprayoon, and P. Boonphayak, "Synthesis of chitosan/brushite powders for bone cement composites," *Journal of the Ceramic Society of Japan,* vol. 116, no. 1349, pp. 36-41, 2008.

[21] M. Rödel, J. Teßmar, J. Groll, and U. Gbureck, "Dual setting brushite—gelatin cement with increased ductility and sustained drug release," *Journal of Biomaterials Applications,* vol. 36, no. 10, pp. 1882-1898, 2022.

[22] S. H. Dabiri, A. Lagazzo, B. Aliakbarian, M. Mehrjoo, E. Finocchio, and L. Pastorino, "Fabrication of alginate modified brushite cement impregnated with antibiotic: Mechanical, thermal, and biological characterizations," *Journal of Biomedical Materials Research Part A,* vol. 107, no. 9, pp. 2063-2075, 2019.
[23] C. Morilla *et al.*, "Effect of the addition of alginate and/or tetracycline on brushite cement properties," *Molecules,* vol. 26, no. 11, p. 3272, 2021.
[24] J. B. Cassel, M. C. Tronco, T. C. Paim, M. R. Wink, and L. A. dos Santos, "Reinforcement of injectable premixed α-tricalcium phosphate cements with silk fibroin solutions," *Materials Today Communications,* vol. 38, p. 108440, 2024.
[25] X.-D. Sun, Y.-L. Zhou, J.-Y. Ren, and F.-Z. Cui, "Effect of pH on the fibroin regulated mineralization of calcium phosphate," *Current Applied Physics,* vol. 7, pp. e75-e79, 2007.
[26] R. Shi *et al.*, "Extrusion printed silk fibroin scaffolds with post-mineralized calcium phosphate as a bone structural material," *International Journal of Bioprinting,* vol. 8, no. 4, 2022.
[27] M.-P. Ginebra, C. Canal, M. Espanol, D. Pastorino, and E. B. Montufar, "Calcium phosphate cements as drug delivery materials," *Advanced Drug Delivery Reviews,* vol. 64, pp. 1090-1110, 2012.
[28] S. Pujari-Palmer, X. Lu, V. P. Singh, L. Engman, M. Pujari-Palmer, and M. K. Ott, "Incorporation and delivery of an organoselenium antioxidant from a brushite cement," *Materials Letters,* vol. 197, pp. 115-119, 2017.
[29] R. Reyes, B. De la Riva, A. Delgado, A. Hernandez, E. Sanchez, and C. Evora, "Effect of triple growth factor controlled delivery by a brushite–PLGA system on a bone defect," *Injury,* vol. 43, no. 3, pp. 334-342, 2012.
[30] Y. M. L. Claudia Morilla, Gastón Fuentes, Amisel Almirall, "Synthesis and evaluation of a collagen–brushite cement as a drug delivery system," *International Journal of Materials Research,* vol. 110, 2019.
[31] D. N. Rockwood, R. C. Preda, T. Yücel, X. Wang, M. L. Lovett, and D. L. Kaplan, "Materials fabrication from Bombyx mori silk fibroin," *Nature protocols,* vol. 6, no. 10, pp. 1612-1631, 2011.
[32] A. Nisal *et al.*, "Silk fibroin micro-particle scaffolds with superior compression modulus and slow bioresorption for effective bone regeneration," *Scientific reports,* vol. 8, no. 1, p. 7235, 2018.
[33] Z. Wang *et al.*, "Dual-functional porous and cisplatin-loaded polymethylmethacrylate cement for reconstruction of load-bearing bone defect kills bone tumor cells," *Bioactive Materials,* vol. 15, pp. 120-130, 2022.
[34] C. Persson and S. Berg, "Strategies towards injectable, load-bearing materials for the intervertebral disc: a review and outlook," *Journal of Materials Science: Materials in Medicine,* vol. 24, pp. 1-10, 2013.
[35] S. Gallinetti, C. Canal, and M. P. Ginebra, "Development and characterization of biphasic hydroxyapatite/β-TCP cements," *Journal of the American Ceramic Society,* vol. 97, no. 4, pp. 1065-1073, 2014.
[36] F. Tamimi *et al.*, "Doxycycline sustained release from brushite cements for the treatment of periodontal diseases," *Journal of Biomedical Materials Research Part A: An Official Journal of The Society for Biomaterials, The Japanese Society for Biomaterials, and The Australian Society for Biomaterials and the Korean Society for Biomaterials,* vol. 85, no. 3, pp. 707-714, 2008.
[37] R. Salomoni, P. Léo, A. Montemor, B. Rinaldi, and M. Rodrigues, "Antibacterial effect of silver nanoparticles in Pseudomonas aeruginosa," *Nanotechnology, science and applications,* pp. 115-121, 2017.
[38] E. M. Tekwu, A. C. Pieme, and V. P. Beng, "Investigations of antimicrobial activity of some Cameroonian medicinal plant extracts against bacteria and yeast with gastrointestinal relevance," *Journal of ethnopharmacology,* vol. 142, no. 1, pp. 265-273, 2012.
[39] B. van Oirschot, A. G. Mikos, Q. Liu, J. J. van den Beucken, and J. A. Jansen, "Fast Degradable Calcium Phosphate Cement for Maxillofacial Bone Regeneration," *Tissue Engineering Part A,* vol. 29, no. 5-6, pp. 161-171, 2023.
[40] P. D. Costantino *et al.*, "Applications of fast-setting hydroxyapatite cement: cranioplasty," *Otolaryngology—Head and Neck Surgery,* vol. 123, no. 4, pp. 409-412, 2000.
[41] F. Roshanfar *et al.*, "Reinforcement of calcium phosphate cement with hybrid silk fibroin/kappa-carrageenan nanofibers," *Biomedicines,* vol. 11, no. 3, p. 850, 2023.
[42] B. Wang, R. J. Xie, Q. Wan, Y. Wang, and Y. Y. Huang, "Effect of silk fibroin on the properties of calcium phosphate cement," *Advanced Materials Research,* vol. 175, pp. 100-104, 2011.

[43] A. Ayyar and N. Chawla, "Microstructure-based modeling of crack growth in particle reinforced composites," *Composites Science and technology,* vol. 66, no. 13, pp. 1980-1994, 2006.
[44] I. Lodoso-Torrecilla *et al.*, "Multimodal porogen platforms for calcium phosphate cement degradation," *Journal of Biomedical Materials Research Part A,* vol. 107, no. 8, pp. 1713-1722, 2019.
[45] J. B. Cassel, M. C. Tronco, B. A. de Melo, F. d. S. de Oliveira, and L. A. Dos Santos, "α-Tricalcium phosphate cement reinforced with silk fibroin: A high strength biomimetic bone cement with chloride-substituted hydroxyapatite," *Journal of the Mechanical Behavior of Biomedical Materials,* vol. 143, p. 105936, 2023.
[46] D. Paul, "Elaborations on the Higuchi model for drug delivery," *International journal of pharmaceutics,* vol. 418, no. 1, pp. 13-17, 2011.
[47] M. Fosca, J. V. Rau, and V. Uskoković, "Factors influencing the drug release from calcium phosphate cements," *Bioactive Materials,* vol. 7, pp. 341-363, 2022.
[48] Z. Dong, D. Wu, H. Engqvist, J. Luo, and C. Persson, "Silk fibroin hydrogels induced and reinforced by acidic calcium phosphate–A simple way of producing bioactive and drug-loadable composites for biomedical applications," *International Journal of Biological Macromolecules,* vol. 193, pp. 433-440, 2021.